Angle dependent molecular dynamics simulation of flux pinning in YBCO superconductors with artificial pinning sites

P. Paturi, M. Malmivirta, T. Hynninen and H. Huhtinen

E-mail: petriina.paturi@utu.fi
Wihuri Physical Laboratory, Department of Physics and Astronomy, University of Turku, Finland

Abstract. A molecular dynamics (MD) simulation to simulate the vortices in superconductors with artificial pinning sites is presented. The simulation reproduces the correct anisotropic behavior in angular dependence of critical current. We also show that the shape of the $J_c(B)$ curve depends on the size of the pinning sites and the change from $p = 0.5$ to $p \approx 1$ is due to the breaking of the vortex lattice to individually acting vortices. The results beautifully correspond to experimental data. Furthermore, we found that the size and shape of the c-axis peak observed with columnar pinning sites in $J_c(\theta)$ also depends on the size of the rods, larger pinning sites leading to wider peaks. The results obtained from the MD-simulation are similar to those of the much more computationally intensive Ginzburg-Landau simulations. Furthermore, the MD-simulations can provide insight to the vortex dynamics within the samples.

PACS numbers:

1. Introduction

Vortex pinning in high temperature superconductors, most often in $YBa_2Cu_3O_{6+x}$ (YBCO), has been under considerable research effort in the last ten years [1]. Applications of superconducting wires typically would need isotropic critical current density, J_c, which is as high as possible. The typical method of increasing J_c and decreasing the intrinsic anisotropy is using artificial pinning centers (APC) which are typically non-superconducting nanoscale inclusions within the matrix of the superconductor. Depending on the growth method, the APCs form columnar nanorods or roughly spherical nanoparticles with diameter of a few nanometers.

The J_c of a superconductor in magnetic field is defined by its capability of pinning vortices as the movement of vortices will cause energy dissipation and a voltage drop. At low magnetic fields, the vortices are widely separated and the main contribution to the total force experienced by the vortex comes from the individual pinning sites. The pinning forces of different kinds of pinning sites have been comprehensively derived by Blatter *et al* [2]. If the pinning sites are weak, collective pinning by them determines the J_c at low fields [3]. Superconductors with only weak pinning sites are not interesting from application point of view, so they will be left out of our study. The strongest pinning sites are columnar rods with diameter of the same order of magnitude as the vortices aligned along the external magnetic field. Large enough rods can also make the vortices align along the rods instead of the external magnetic field, leading to the well known c-axis peak observed in *e.g.* $BaZrO_3$ doped YBCO made by pulsed laser deposition [4].

At higher magnetic fields, the vortices are closer to each other and the repulsive vortex-vortex interaction will effectively reduce the pinning force of the pinning sites. This leads to the reduction of J_c with increasing magnetic fields. If the pinning sites are very strong, they will break the triangular Abrikosov vortex lattice, which is formed with weak pinning sites, and each vortex is still individually pinned. In the other extreme, the pinning sites will not be able to break the lattice and the J_c will depend on the stiffness of the vortex lattice and the distribution of pinning sites [5].

In this paper, we present a molecular dynamics (MD) simulation of vortices in pinning landscapes, which do not fulfil the requirements for analytical solutions. This also enables us to look at the angular dependence of J_c ($J_c(\theta)$) with different types and orientations of pinning sites. Here θ is the angle between the external magnetic field and the c axis of YBCO. The angular dependence has been modelled using statistical approach on the paths of the vortices [6, 7, 8] assuming different orientations and distributions of pinning sites. Unfortunately, the statistical approach does not really give microscopic information on the optimal pinning sites, even though it helps to understand the forms of the $J_c(\theta)$ curves.

In this paper we show that the MD simulation can reproduce the correct anisotropic behavior of J_c with isotropic pinning sites. In addition, we show that the behavior of $J_c(B)$ changes with the size of the pinning centers in accordance with experimental

data and that the size of the pinning centers is also a determining factor in $J_c(\theta)$. The simple MD simulations also reproduce results obtained earlier with Ginzburg-Landau simulations and give insight to the vortex dynamics in the superconductors, which the GL-simulations do not give. With thorough understanding, real design-based superconductors can be made.

2. Methods

2.1. Molecular dynamics simulations

We simulate vortices using a simplified MD model, where each vortex is represented by a chain of particles. In addition to the vortices, pinning sites are also explicitly included in the simulation as particles, but the YBCO lattice itself is not. Pinning sites are immobile, and only the particles representing vortices are allowed to move during the simulation. Dynamics are implemented using the leapfrog version of the velocity-Verlet algorithm .

The simulations are three-dimensional, but we split the simulation into layers perpendicular to the YBCO c axis to enhance computational efficiency. This means that the particles representing vortices are restricted to move only in these ab layers, and motion in the c direction is not allowed. A vortex is represented by a chain of particles so that each layer contains exactly one particle. Particles in adjacent layers are connected by a spring-like force representing the line tension of the vortex. Particles belonging to different vortices only interact if they are in the same layer. Similarly, vortex particles only interact with pinning sites which are in the same layer. The only interaction between layers is the line tension in a vortex. A schematic picture of the simulation configuration is shown in Fig. 1.

Pinning sites have different interaction radii representing their pinning strength. Columnar pinning sites are constructed in a similar fashion as the vortices: a column is represented by a stack of particles where each layer holds exactly one particle.

We apply periodic boundary conditions in the simulation layers, i.e, the YBCO ab plane. However, we have free boundaries in the c direction. This means that the simulation is periodically infinite in the ab plane but finite in the c direction. This models the thin film geometry generally used in YBCO superconductors.

We also include an external magnetic field in the simulation, and the direction of the magnetic field with respect to the c axis is adjustable. Vortices tend to align themselves in the direction of the external magnetic field, and this introduces anisotropy in the simulation. The layered structure of the simulation assumes that the vortices run approximately in the c direction, and thus magnetic fields nearly perpendicular to the c axis are incompatible with the layered model. This limits the range of magnetic field angles we are able to study.

The total force acting on particle i (in layer i) of vortex n is

$$\mathbf{F}^{\mathrm{tot}}_{(i,n)} = \sum_{m\neq n} \mathbf{f}^{\mathrm{vv}}_{(i,n),(i,m)} + \sum_{k} \mathbf{f}^{\mathrm{vp}}_{(i,n),(i,k)} + \sum_{j=i\pm1} \mathbf{f}^{\mathrm{tension}}_{(i,n),(j,n)} + \sum_{j=i\pm1} \mathbf{f}^{\mathrm{magnetic}}_{(i,n),(j,n)} + \mathbf{f}^{\mathrm{Lorentz}}_{(i,n)} + \mathbf{f}^{\mathrm{drag}}_{(i,n)}. \quad (1)$$

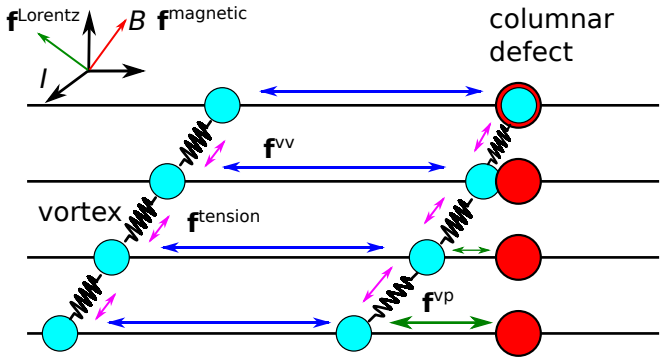

Figure 1. A schematic diagram of the used molecular dynamics model. Vortices are turquoise and pinning sites red. The particles of a vortex are connected with a spring-like force. For visualisation, only four layers are shown. Interactions are shown with arrows.

Here $\mathbf{f}^{\mathrm{vv}}_{(i,n),(i,m)}$ is the force between the particles of vortices n and m in layer i. The force $\mathbf{f}^{\mathrm{vp}}_{(i,n),(i,k)}$ is due to the interaction between the particle of vortex n in layer i and the pinning site k in the same layer. Vortex line tension is represented by $\mathbf{f}^{\mathrm{tension}}_{(i,n),(j,n)}$, and this force acts between particles of the same vortex n which are in adjacent layers i and j. The tendency of the vortex to orient itself along magnetic field lines is driven by the force $\mathbf{f}^{\mathrm{magnetic}}_{(i,n),(j,n)}$. This force depends on the orientation of the vortex, and thus it is a function of the positions of vortex particles in adjacent layers. Next, $\mathbf{f}^{\mathrm{Lorentz}}_{(i,n)}$ is the Lorentz force caused by the transport current and the magnetic field, and finally, $\mathbf{f}^{\mathrm{drag}}_{(i,n)}$ is the drag force that vortices experience in superconductors.

The magnitude of the vortex-vortex force is [9, 10]

$$f^{\mathrm{vv}} = \frac{\epsilon_0}{\lambda_{ab}} \mathrm{K}_1\left(\frac{r}{\lambda_{ab}}\right), \tag{2}$$

where ϵ_0 is the characteristic vortex energy per length, λ is the magnetic penetration depth, $r = r_{(i,n),(i,m)}$ is the in-layer distance between two vortex particles, K_1 is the Bessel function of first kind, first order. The characteristic energy is $\epsilon_0 = \phi_0^2/(2\pi\mu_0\lambda^2) \approx 2.76 \cdot 10^{11}$ J/m, where ϕ_0 is the magnetic flux quantum and μ_0 the magnetic permeability of free space.

The force between a vortex and a pinning site is [11, 2]

$$f^{\mathrm{vp}} = \epsilon_0 \frac{r r_0^2}{(r^2 + 2\varepsilon_\vartheta \xi_{ab}^2)^2}, \tag{3}$$

where $r = r_{(i,n),(i,k)}$ is the in-layer distance between a pinning site and a vortex, r_0 the radius of the pinning site and ξ the coherence length of YBCO and ε_ϑ is the angle-dependent Blatter scaling parameter[2]

$$\varepsilon_\vartheta^2(\theta) = \frac{\sin^2\theta}{\gamma^2} + \cos^2\theta, \tag{4}$$

where θ is the angle between the external magnetic field and the axis along the c lattice parameter direction and γ is the anisotropy parameter of YBCO (≈ 5.0). The pinning

site radius was varied in range 0.1 – 6 nm in the simulations. Although, Eq. (3) is strictly speaking valid only for pinning sites sizes smaller than $r_0 < \sqrt{2}\xi$, the error done in comparison to the force obtained for large pinning sites [2] is small. At large distances the two equations give asymptotically the same force. The small pinning site force, Eq. (3), is also numerically stable unlike the large pinning site force, which diverges near the pinning site.

Vortex line tension energy is [2, 12]

$$e^{\text{tension}} = \epsilon_0 \varepsilon_\vartheta L \ln \frac{\lambda}{\varepsilon_\vartheta \xi}, \tag{5}$$

where L is the length of a vortex. Taking the derivative of this energy with respect to the separation $\Delta\mathbf{r} = \mathbf{r}_{(i,n)} - \mathbf{r}_{(j,n)}$ between adjacent vortex particles, one finds the line tension force. In our layered simulation, where the vortex particles are only allowed to move in the ab plane, we only need the component of this force in this plane. The magnitude of this component is

$$f^{\text{tension}} = -\frac{\epsilon_0 r(\gamma^2 - 1 + \ln\kappa)}{d\gamma^2\sqrt{d^2 + r^2}}, \tag{6}$$

where $d = \Delta r_c = r_{c,(i,n)} - r_{c,(j,n)}$ is the distance between adjacent vortex particles in the c direction (i.e., the distance between adjacent layers in the simulation) and $r = \Delta r_{ab} = r_{ab,(i,n)} - r_{ab,(j,n)}$ is the distance between the particles in the ab plane. The constant κ is the Ginzburg-Landau parameter (100 for YBCO).

The energy of a vortex in an external magnetic field, $\mathbf{B}_{\text{ext}}$, tilted at an angle φ with respect to the field, is

$$e^{\text{magnetic}} = -\phi_0 \mu_0 B_{\text{ext}} \cos\varphi. \tag{7}$$

Differentiating this yields the force

$$f^{\text{magnetic}} = \phi_0 \mu_0 B_{\text{ext}} \sin\varphi \frac{\mathrm{d}\varphi}{\mathrm{d}r}. \tag{8}$$

The Lorentz force is $f^{\text{Lorentz}} = \phi_0 |\hat{\mathbf{B}}_{\text{ext}} \times \mathbf{J}_{\text{c}}| = \phi_0 J_{\text{c}}$. The equality holds true because the current is always kept perpendicular to the magnetic field.

The drag force resist vortex movement, and so it is always opposite to the velocity $\mathbf{v}$ of a vortex particle,

$$\mathbf{f}^{\text{drag}} = -\eta \mathbf{v}. \tag{9}$$

The drag coefficient η is [13]

$$\eta = \frac{\phi_0 B_{\text{c2}}}{\rho_n}, \tag{10}$$

where ρ_n is the normal state resistivity of YBCO[14], $5.3 \cdot 10^{-7}$ Ωm and the upper critical field[15], B_{c2}, is 27 T at 77 K in the c direction.

The drag force is dissipative and its inclusion removes energy from the simulation. Therefore the drag force acts effectively like a Langevin thermostat set to 0 K. If the vortices are pinned, the drag force will remove energy from the simulation until the

vortices are completely stationary. If the vortices are not pinned, work done by the Lorentz force adds energy in the simulation, accelerating the motion of the vortices. In this case, a steady state is eventually reached, where the work done by the Lorentz force is cancelled by the negative work done by the drag force and the vortices travel on average at constant velocity.

In our simulations, we are most interested in distinguishing between the state of pinned vortices and the state of traveling vortices in order to estimate the critical current. The exact temperature of the system can affect the tendency of vortices to get pinned, but in our current simulation we merely assume that the temperature is low and do not apply a thermostat set to a finite temperature.

The MD model also requires that vortex particles have a mass and vortices with different masses can behave differently[16]. In this study, we have used a mass of 10^{20} kg. This value is somewhat arbitrary, but according to our test calculations, our results do not depend on the precise value of this mass. This is because the timescale of the simulation is defined by how quickly the vortices reach the steady state where they travel at constant velocity. The characteristic time, τ, for this process is given by the ratio of the vortex mass and the drag coefficient, and since $\eta \approx 10^{-7}$ kg/s, a mass of 10^{-20} kg gives $\tau = m/\eta \approx 10^{-13}$ s. The distance between pinning sites is roughly 10^{-7} m and the terminal velocity of vortices, which depends on the Lorentz and drag forces but not the vortex mass, can go up to 10^3 m/s. Therefore, vortex travel time from one pinning site to another is about 10^{-10} s. This is 1000 times longer than the characteristic time τ, which means that the vortices reach their terminal velocity very quickly and travel at constant speed. This result is true as long as τ is clearly smaller than the travel time between pinning sites, and as long as the mass is in this regime, vortex dynamics do not depend on the exact value of the mass.

2.2. Simulated systems

The pinning landscapes (pinscapes) contained either nanorods or single nanodots of different sizes. The distribution of the nanorods in the simulations were randomly generated so that there is a minimum distance ($\approx$ 20 nm) between the rods. This was to ensure that the pinscape was as close to the experimentally observed as possible (e.g. BZO rods in YBCO). The positions of the nanodots were randomly generated in each layer. In each simulation run several (4–15) pinscapes were used and the results averaged. The error bars represent the mean error as calculated from these simulations.

The number of vortices in the simulation was determined by the field strength according to equation $B = n\phi_0$, where n is the vortex density. The size of the calculation area was varied from 200×200 nm^2 to 400×400 nm^2. The larger systems were used at low fields where vortex density is lower. The used magnetic field range was 0.1 – 2.0 T.

The critical current was iterated by the bisection method. The simulation was run with one current and the current in the following iteration was adjusted according to

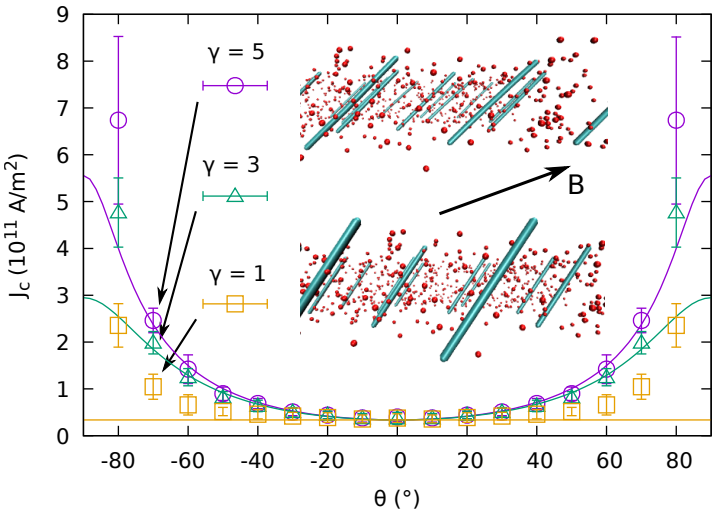

Figure 2. $J_c(\theta)$ curves calculated for different anisotropy constants γ. The points are the simulation results and the curves show the theoretical dependences. The insets show examples of vortex configurations (blue rods) in the pinscape formed by isotropic pinning centers (red spheres) at magnetic field angle of -70° for the $\gamma = 5$ (top) and $\gamma = 1$ (bottom) points. The B arrow shows the direction of the external field.

the stability of the system. The average of the vortex position was calculated over all the layers. Additionally, if this condition was not fulfilled, the average speed of the vortices was checked. A vortex was considered pinned if its current speed was below a defined limit. As the speed of a vortex is defined by the arbitrarily chosen vortex particle mass, the speed limit is also arbitrary. In low fields, a lower speed limit was used, since the force caused by the field is so small that the vortices were practically always stable. Both the position and speed stability were checked with regular intervals during the simulation.

3. Simulation results and comparison to experimental data

3.1. Anisotropy

The validity of the anisotropic corrections to the line tension force (Eq. (5)) and the vortex-pinning site force (Eq. (3)) was checked by running simulations with random isotropic spherical pinning sites and different anisotropy constants γ. The results for $\gamma = 1$, 3 and 5 with theoretical curves (Eq. (4)) for each are shown in Fig. 2. It is clearly seen that at high angles the simulation does break up, but it represents reality fairly well up to 60 degrees with YBCO's $\gamma = 5$. With lower anisotropy the simulation results start deviating from the theoretical curve at lower angles. The breaking of the model is due to the layered nature of the simulation, where at high angles the vortices lie almost along the *ab*-planes and still do not interact through the layers. Fixing this would require a real 3 dimensional simulation with interactions between all the vortices and pinning sites.

The insets of Fig. 2 show representative stable vortex configurations at external field angle of -70 degrees. The different anisotropies of the superconductors are visible in the angles of the vortices seen in the images of the vortex configurations: higher the anisotropy more slanted the vortex is. The angle of the vortex is defined by two competing forces. The external magnetic field tries to align the vortex with itself, whereas the line tension tends to shorten the vortex and thus turn it more along the thinnest direction of the superconductor. In high anisotropy superconductors the vortices are more flexible along the planes, thus the vortices are more along the external field with $\gamma = 5$.

3.2. Rod size dependence of $J_c(B)$

Curving of the $J_c(B)$ dependence in log-log graphs [17] is a typical feature of YBCO thin films with APC's. In pure YBCO films, $J_c(B)$ is nicely described with $B^{-\alpha}$, where α is around 0.5 at low temperatures. In APC films, on the other hand, a smooth curving of $J_c(B)$ is observed and determination of α is fairly arbitrary, but generally in range 0.1–0.4 [18, 19, 20]. Instead of $J_c(B)$, many authors have calculated the pinning force $F_p = |\mathbf{J}_c \times \mathbf{B}| = J_c B$ in the maximum Lorentz force configuration, where J_c and B are always kept perpendicular. The shape of F_p has been derived by e.g. Dew-Hughes[21] and Kramer [22] to be

$$F_p(B) = F_{p0} \left(\frac{B}{B_{c2}} \right)^p \left(1 - \frac{B}{B_{c2}} \right)^q , \tag{11}$$

where F_{p0} scales the pinning force at maximum, B_{c2} is the upper critical field and p and q are exponents which depend on the type of pinning sites in the sample. In the model by Dew-Hughes for non-magnetic pinning sites, if the diameter d is much smaller than the coherence length ξ, $p = 0.5$ and if $d \gg \xi$, $p = 1$. In high-temperature superconductors B_{c2} has been replaced by B_{irr} [23], as in them B_{irr} marks the limit above which J_c is zero. We have recently suggested scaling the field with the magnetic field value at maximum force, B_{max} to enable reliable fitting of Eq. (11) [17]. It is immediately seen that in the first order approximation $\alpha = 1 - p$ and the curvature at high field is mostly determined by q. The value of q can be derived from Ginzburg-Landau (GL) theory to be $q = 1$[17], but if derived from the shear modulus c_{66} of the vortex lattice, value $q = 2$ is often obtained[5, 24]. Also statistical variation of the pinning site sizes changes q[25].

To understand the change in the shape of $J_c(B)$, we simulate systems containing columnar rods of different radii as pinning sites. Fig. 3 shows the dependence of the scaled pinning force F_p for a 4-wt% BZO- and BCO-doped YBCO films[26, 27], as well as simulations of 3 nm and 6 nm diameter rods,. The inset shows the measured and simulated $J_c(B)$ dependeces. The simulated values have been shifted to fit the experimental data at one field value, but the field dependence has not been changed. A clear difference is seen between the different sizes of pinning sites. On the right of the figure, the stable simulation states are shown for 6 nm and 3 nm rods at critical current in field of 0.75 T, which is below the accommodation field. Even so, only a few

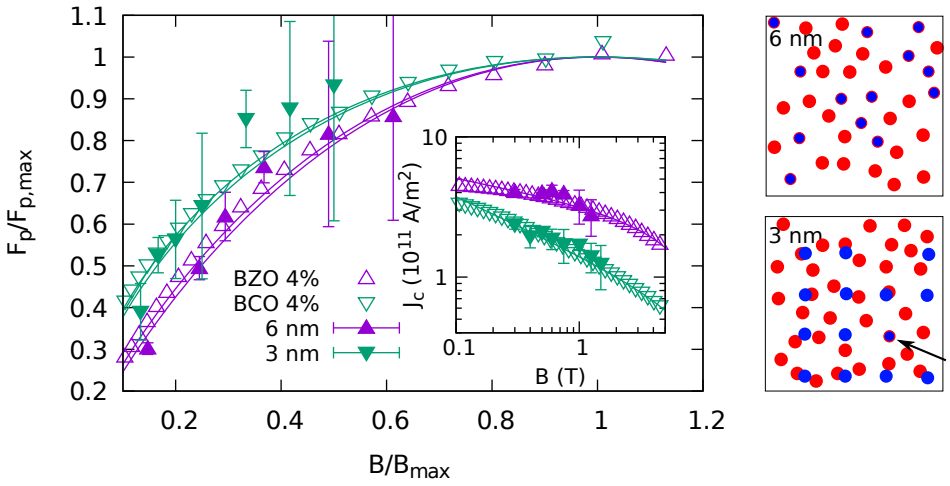

Figure 3. Scaled pinning forces for 4 wt-% BZO- and BCO-films together with the simulated values for corresponding pinning site sizes (diameters 3 nm and 6 nm). The inset shows the measured J_c values as function of external magnetic field. The simulation J_c values have been shifted to fit the experimental data on the lowest field value. On the right are shown the stable states of the simulations at critical current at 0.75 T. The arrow shows the one pinned vortex in the vortex lattice.

of the vortices are pinned into the small diameter rods, and the rest are stabilized by the vortex-vortex interaction to a lattice. This leads to fast degradation of the critical current with field. When the pinning sites are large, each vortex is individually pinned, the lattice is destroyed and the decrease of the critical current is much slower. The difference of vortex dynamics for different pinning site sizes is clearly visible in the videos available as supplementary information.

The $F_p(B)$ fit was made for simulation results obtained for pinning site sizes varying from 0.5 nm to 14 nm, similarly as in Fig. 3. To ease the fitting, q was fixed to 1.1 [17] for all the sizes. First the scaling with $F_{p,max}$ and B_{max} was done and then p fitted. The fitted p values are shown in Fig. 4 together with experimental data on different kinds of YBCO films[17] and Ginzburg-Landau simulations [28]. It is clearly seen that the MD-simulations follow the same size dependence for p as the experimental data and the GL-simulations. When the pinning sites are small, such as dislocations, $p = 0.5$ as expected from the Ginzburg-Landau theory. With small pinning sites, the vortex-vortex interactions are comparable to the vortex-pinning site interactions, which leads to the vortex lattice staying in tact, as also seen in the supplementary videos. When the pinning sites are large ($d \gg \xi$), we get $p \approx 1$, as also expected from the Ginzburg-Landau theory. In this case the pinning force from the pinning sites is so large that it breaks the vortex lattice.

Between the extremes of small pinning sites and large pinning sites, it is natural that p changes smoothly. In these cases the vortex lattice is still somewhat intact, but distorted. This range is difficult to reach analytically. It should be noted that the current MD-simulations also reproduce the much more complicated GL-simulations

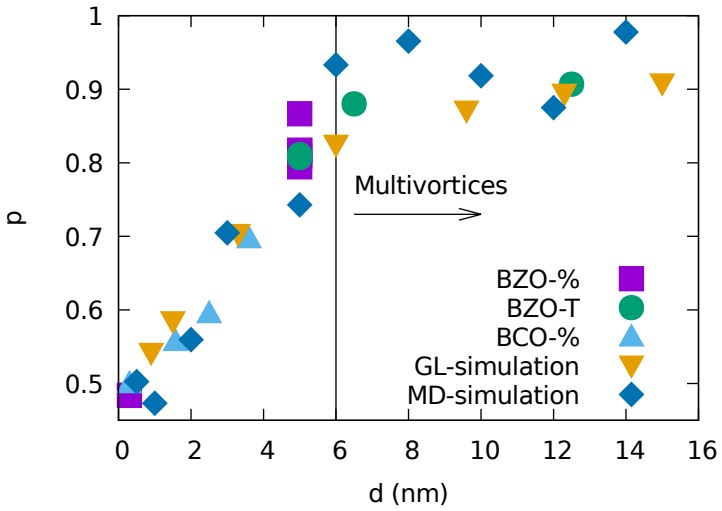

Figure 4. The dependence of p on the size of the pinning site. BZO-% refers to samples with different BZO-doping[26], BZO-T to samples made at different temperatures [29] and BCO-% to samples with different BCO content[27]. The vertical line shows the limit above which multivortices were observed in the GL-simulations.

and that in addition *e.g.* the breaking of the vortex lattice is easily observed in the MD-simulation.

From these results, we can also conclude that the optimal diameter of pinning sites is actually quite close to 4ξ, where p reaches ≈ 1 (around 10 nm at low temperature for YBCO). Above this size the field dependence does not change and in the GL-simulations multivortices are seen[28]. If the pinning site diameter is further increased the superconducting cross section of the sample decreases and thus the critical current density starts to decrease. It has also been observed that adding second phase pinning sites tends to decrease the zero or self field critical current density [14, 26, 30]. This can be understood as increase of the magnetic field penetration depths λ due to the decrease of the superconducting energy gap [31, 32]. The lattice distortions caused by the dopants diminish the energy gap. This is also seen as the general trend of decreasing T_c with increasing doping [14, 33]. Therefore limiting the doping to minimum is necessary. The optimal density of pinning sites depends on the magnetic field used in the intended application.

3.3. Angular dependence of J_c in films with different rod sizes

In superconducting applications the goal is to have as high and isotropic $J_c(\theta)$ as possible. To that end nanorods have been introduced as pinning sites. These produce a wide peak in $J_c(\theta)$ in the direction of the rod. The actual shapes of $J_c(\theta)$ depend on e.g. diameter, length and orientation of the rods as well as on temperature and magnetic field. In addition, all real films contain dislocations and twin boundaries, which affect pinning, specially at low temperatures.

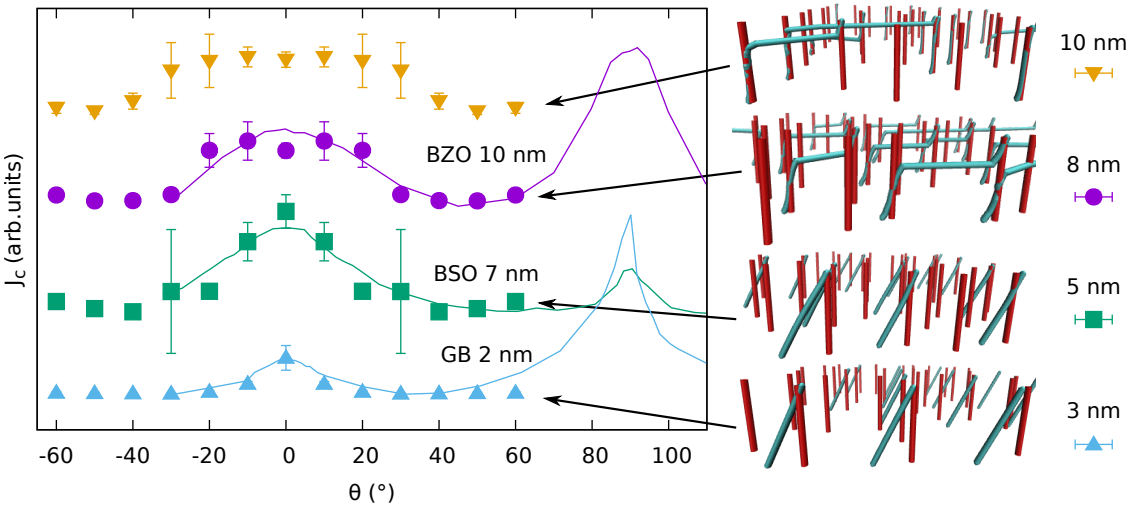

Figure 5. The simulation results for angle dependent J_c for samples with different diameter direct nanorods (10, 8, 5 and 3 nm). On the right are vortex configurations at the critical current with magnetic field angle of 30°. The lines in the left panel are experimental data: BZO is from $BaZrO_3$ doped YBCO films with nanorod diameter around 10 nm (Kang et al[34]), BSO from $BaSnO_3$ doped YBCO films with nanorod diameter around 7 nm (Horide et al[35]) and GB from YBCO film on Hastelloy substrate with low angle grain boundaries (Wee et al [36]).

In order to study the effect of rod sizes to the angular dependence, simulations were run at 0.75 T for rods without any splay. Fig. 5 shows the $J_c(\theta)$ results for nanorods with different diameters along with representative vortex configurations in the simulation at 30°angle. It is clearly seen that as the nanorod diameter increases and the pinning force of the rod increases, the rod is capable of holding segments of vortex along it. When the magnetic field angle is too high compared to the pinning force of the rod, the rods act as point pinning sites and vortices follow the external field. The observed J_c is higher when larger segments of the vortex are pinned. The angle of change between these modes depends on the rod diameter and thus determines the width of the observed c-axis peak. The normal anisotropic curve is obtained when the pinning sites are not strong enough to make the vortices follow them. Animations of the simulations are available as supplementary material.

To compare the simulated $J_c(\theta)$ with experiments, we took previously published $J_c(\theta)$ data from three different kinds of samples. These were $BaZrO_3$ doped film [34] with 10 nm rods, $BaSnO_3$ doped film [35] with 7 nm rods and an YBCO film on Hastelloy substrate [36], which had low angle grain boundaries ($\Delta\phi = 3°$). The low angle grain boudaries are assumed to be distorted areas around dislocations and thus a few nanometer wide. All the data has been taken at 77 K and 1 T, which are readily available in the literature. The field is close to the one used in the simulation and at this temperature the twins and normal dislocations are fairly ineffective thus the pinscape better corresponds to the simple one used in the simulation. The data are shown as

lines in Fig. 5 and the qualitative agreement is good. The discrepancies at the widths of the c-axis peaks are explained by splay of the rods in the real samples, the other pinning sites in the samples and the small scale of the simulations.

4. Conclusions

In this work we have made a molecular dynamics simulation to simulate the vortices in superconductors with artificial pinning sites. We have shown that the simulation reproduces the correct anisotropic behavior in angular dependence of critical current. We also showed that the shape of the $J_c(B)$ curve depends on the size of the pinning sites and the change from $p = 0.5$ to $p \approx 1$ is due to the breaking of the vortex lattice to individually acting vortices. The results beautifully correspond to experimental data. Furthermore, we found that the size and shape of the c-axis peak observed with columnar pinning sites in $J_c(\theta)$ also depends on the size of the rods, larger pinning sites leading to wider peaks. This is a consequence of the large pinning force of the large pinning sites, which can stretch the vortices from one pinning site to another. The results obtained from the MD-simulation are similar to those of the much more computationally intensive GL-simulations. Furthermore, the MD-simulations can provide insight to the vortex dynamics within the samples. Thus, we conclude that the very simple MD model can be used to understand and predict $J_c(B)$ and $J_c(\theta)$ behavior of YBCO superconductors.

Obvious improvements to be done in the future are including temperatures higher than 0 K. The layered simulation presented here is computationally efficient, but it cannot represent systems where the external magnetic field is oriented close to the ab plane. Especially, we cannot simulate the experimentally observed ab peaks using this model. We plan to fix this shortcoming by extending the layered simulation to a full three-dimensional model.

Acknowledgments

The Jenny and Antti Wihuri Foundation is acknowledged for financial support and M.M. acknowledges also the Finnish Cultural Foundation. The computer resources of the Finnish IT Center for Science (CSC) and the FGCI project (Finland) are also acknowledged.

Bibliography

[1] Matsumoto K and Mele P 2010 *Supercond. Sci. Technol.* **23** 014001
[2] Blatter G, Feigel'man M V, Geshkenbein V B, Larkin A I and Vinokur V M 1994 *Reviews of Modern Physics* **66** 1125–1388
[3] Blatter G, Geshkenbein V B and Koopmann J A G 2004 *Phys. Rev. Lett.* **92** 067009
[4] Paturi P, Irjala M and Huhtinen H 2008 *J. Appl. Phys.* **103** 123907
[5] Ullmaier H 1975 *Irreversible properties of type II superconductors* (Springer-Verlag Berlin Heidelberg)
[6] Long N J 2008 *Supercond. Sci. Technol.* **21** 025007

[7] Wimbush S and Long N 2012 *New J. Phys.* **14** 083017
[8] Paturi P 2010 *Supercond. Sci. Technol.* **23** 025030
[9] Assi H, Chaturvedi H, Dobramysl U, Pleimling M and Täuber U C 2016 *Molecular Simulation* **42** 1401–1409
[10] Brandt E H 1986 *Phys. Rev. B* **34** 6514–6517
[11] Pan V, Cherpak Y, Komashko V, Pozigun S, Tretiatchenko C, Semenov A, Pashitskii E and Pan A V 2006 *Phys. Rev. B* **73** 054508
[12] Balatskii A, Burlachkov L and Goŕkov L 1986 *JETP* **63** 866
[13] Bardeen J and Stephen M J 1965 *Phys. Rev.* **140** A1197–A1207
[14] Malmivirta M, Palonen H, Inkinen S, Yao L D, Tikkanen J, Huhtinen H, Jha R, Awana V P S, van Dijken S and Paturi P 2016 *J. Phys. Cond. Mat.* **28** 175702:1–6
[15] Sekitani T, Miura N, Ikeda S, Matsuda Y H and Shiohara Y 2004 *Phys B* **346-347** 319
[16] de Vondel J V, de Souza Silva C C, Zhu B, Morelle M and Moshchalkov V 2005 *Phys. Rev. Lett.* **94** 057003
[17] Paturi P, Malmivirta M, Palonen H and Huhtinen H 2016 *IEEE T. Appl. Supercond.* **26** 8000705
[18] Mele P, Matsumoto K, Ichinose T H A, Mukaida M, Yoshida Y and Horii S 2007 *Supercond. Sci. Technol.* **20** 244
[19] Feldmann D M, Holesinger T G, Maiorov B, Foltyn S R, Coulter J Y and Apodaca I 2010 *Supercond. Sci. Technol.* **23** 095004
[20] Goyal A, Kang S, Leonard K J, Martin P M, Gapud A A, Varela M, Paranthaman M, Ijadoula A O, Specht E D, Thompson J R, Christen D K, Pennycook S J and List F A 2005 *Supercond. Sci. Technol.* **18** 1533–1538
[21] Dew-Hughes D 1974 *Philosophical magazine* **30** 293
[22] Kramer E J 1973 *J. Appl. Phys.* **44** 1360
[23] Barilo S N, Shiryaev S V, Gatalskaya V I, Lynn J W, Baran M, Szymczak H, Szymczak R and Dew-Hughes D 1998 *Phys. Rev. B* **58** 12355
[24] Matsushita T 2007 *Flux pinning in superconductors* (Springer, Heidelberg, Germany)
[25] Cooley L D, Stejic G and Larbalestier D C 1992 *Phys. Rev. B* **46** 2964
[26] Huhtinen H, Irjala M, Paturi P, Shakhov M A and Laiho R 2010 *J. Appl. Phys.* **107** 053906
[27] Malmivirta M, Yao L D, Inkinen S, Huhtinen H, Palonen H, Jha R, Awana V P S, van Dijken S and Paturi P 2015 *IEEE T. Appl. Supercond.* **25** 6603305:1–5
[28] Palonen H, Jäykkä J and Paturi P 2012 *Phys. Rev. B* **85** 024510
[29] Malmivirta M, Yao L, Huhtinen H, Palonen H, van Dijken S and Paturi P 2014 *Thin Solid Films* **562** 554–560
[30] Irjala M, Huhtinen H, Jha R, Awana V P S and Paturi P 2011 *IEEE Trans. Appl. Supercond.* **21** 2762–2766
[31] Talantsev E F and Tallon J L 2015 *Nature Communications* **6** 7820
[32] Talantsev E F, Crump W P and Tallon J L 2017 *Scientific reports* **7** 10010
[33] Peurla M, Paturi P, Stepanov Y P, Huhtinen H, Tse Y Y, Bódi A C, Raittila J and Laiho R 2006 *Supercond. Sci. Technol.* **19** 767–771
[34] Kang S, Leonard K J, Martin P M, Li J and Goyal A 2007 *Supercond. Sci. Technol.* **20** 11
[35] Horide T, Kawamura T, Matsumoto K, Ichinose A, Yoshizumi M, Izumi T and Shiohara Y 2013 *Supercond. Sci. Technol.* **26** 075019
[36] Wee S H, Zuev Y L, Cantoni C and Goyal A 2013 *Sci. Rep.* **3** 23101–9